

## Bias characteristics in the AVHRR sea surface temperature

Huai-Min Zhang, Richard W. Reynolds, and Thomas M. Smith

NOAA NESDIS National Climatic Data Center, Asheville, North Carolina, USA

Received 10 October 2003; accepted 18 December 2003; published 13 January 2004.

[1] To provide possible means to improve future satellite SST retrieval algorithms and to provide data users with error information, spatiotemporal bias patterns in the 1982–2002 NOAA operational AVHRR SST were characterized. At the start of one (NOAA-14) satellite mission, typical global average biases were about  $-0.05^{\circ}\text{C}$ , and gradually increased during the satellite mission. Normally global averages rarely exceeded  $0.2^{\circ}\text{C}$ , due to cancellation of larger biases of opposite signs in different regions. Biases were inhomogeneous and locally exceeded  $0.5^{\circ}\text{C}$  even in the 21-year time mean. Large irregular biases were due to stratospheric aerosols from volcanic eruptions. Seasonal biases were strongly related to local weather phenomena, such as seasonal dust aerosols and cloud covers. The findings suggest that future satellite SST retrieval algorithms should be time and space dependent. *INDEX TERMS*: 1640 Global Change: Remote sensing; 4215 Oceanography: General: Climate and interannual variability (3309); 4504 Oceanography: Physical: Air/sea interactions (0312); 4275 Oceanography: General: Remote sensing and electromagnetic processes (0689); 4294 Oceanography: General: Instruments and techniques. *Citation*: Zhang, H.-M., R. W. Reynolds, and T. M. Smith (2004), Bias characteristics in the AVHRR sea surface temperature, *Geophys. Res. Lett.*, 31, L01307, doi:10.1029/2003GL018804.

### 1. Introduction

[2] Sea surface temperature (SST) data are widely used to study earth's climate changes, although theoretically heat content is more appropriate. SST is also used in real-time applications, such as boundary conditions for operational numerical forecasts and in data assimilations for the analyses of weather, ocean and climate.

[3] SST has been continuously monitored using the Advanced Very High Resolution Radiometers (AVHRR) on board the U.S. National Oceanic and Atmospheric Administration (NOAA) polar-orbiting satellites since late 1981. Other SST products include those from the Tropical Rainfall Measuring Mission (TRMM) Microwave Imager (TMI; [Kummerow *et al.*, 1998; Wentz *et al.*, 2000]), the Along Track Scanning Radiometer (ATSR; [Mulrow *et al.*, 1994]), and the Moderate Resolution Imaging Spectroradiometer (MODIS; [Esaias *et al.*, 1998]). Satellite SST is not directly measured, but deduced from directly measured parameters (e.g., AVHRR radiances). The deductions may be based on semi-empirical formulae obtained from correlation studies. The AVHRR satellite "brightness" temperatures are usually regressed against selected in situ observations to produce "bulk" SSTs, despite that infrared AVHRR SSTs physically represent only a very thin ( $\sim 10\ \mu\text{m}$ ) ocean skin

layer due to sea water's high emissivity [Emery *et al.*, 2001b; Donlon *et al.*, 2002]. Tuning to the bulk SST is done for historical reasons and for lack of skin SST measurements. Also, because the skin layer is so thin, the bulk SST representing the ocean mixed layer is more suitable for climate study than skin and diurnal SSTs. Thus we focus on the AVHRR SSTs calibrated to bulk SSTs.

[4] Many factors can affect satellite SST accuracy, including orbit and sensor stability, and variations and types of clouds, water vapor and aerosol concentrations in the atmosphere [e.g., Brown *et al.*, 1993; Mulrow *et al.*, 1994]. Although great care was exercised in developing and calibrating the satellite SST algorithms, they were done over limited areas, under limited atmospheric conditions, and for particular conditions of satellite sensors and tracks [e.g., Walton *et al.*, 1998]; (<http://www2.ncdc.noaa.gov/docs/podug/>). Thus spatiotemporal biases still existed. Adjustments to operational algorithms were delayed in time following volcanic eruptions (e.g., Mt. Pinatubo erupted in June 1991 with biases appearing in July. The operational corrections were implemented from early October 1991). Figure 1 shows the AVHRR SST biases in September 1991, with maximum biases larger than  $2^{\circ}\text{C}$ . Here the AVHRR SST biases are statistically characterized. The findings should be useful for improving satellite SST algorithms for retroactive analysis and for future satellite SST missions.

### 2. Data and Method

[5] The NOAA operational AVHRR SST observations started in late 1981 and are continuing into the future. Over the years the SST retrieval algorithms have evolved, from the early Multi-Channel SST (MCSST) algorithm to the cross-product SST algorithm and to the nonlinear SST (NLSST) algorithm [McClain *et al.*, 1985; Walton, 1988; Walton *et al.*, 1998; May *et al.*, 1998]. In situ SSTs have been measured by ships and drifting and moored buoys. The history of in situ SST measurements and analyses was discussed by Kent *et al.* [1993 and 1999], Emery *et al.* [2001a], and Reynolds *et al.* [2002]. To reduce random and sampling errors in both in situ and satellite data, we use an objective analysis method to compute analyzed SST on a spatial grid of  $1^{\circ} \times 1^{\circ}$  monthly. Reynolds and Smith [1994] and Reynolds *et al.* [2002] described the optimum interpolation (OI) in details. The AVHRR SST biases are referenced to in situ SSTs. This is done by an optional Poisson procedure completed prior to the OI analysis. The Poisson step removes satellite SST biases with respect to the in situ SSTs [Reynolds and Smith, 1994]. To extract the AVHRR SST biases, OIs with and without the bias correction (*bc*) were done. The corresponding OI SSTs are denoted as  $T_{bc}$  and  $T_{no.bc}$ . Since satellite SST observations overwhelm in situ data, the influence of in situ SSTs

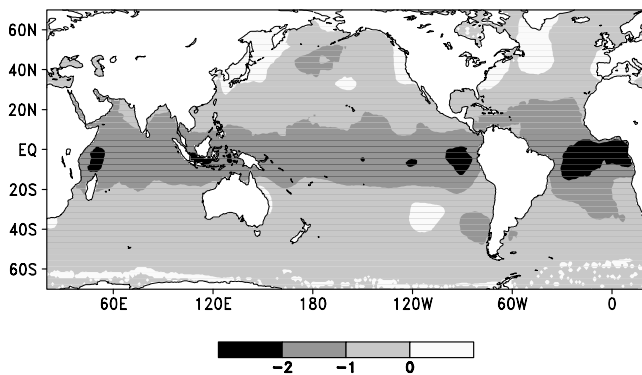


**Figure 1.** September 1991 AVHRR SST biases ( $^{\circ}\text{C}$ ) following the Mt. Pinatubo eruption. The biases are computed using the method described in Section 2.

on the OI SSTs without the bias correction is minimal. Therefore we define the AVHRR SST bias,  $B$ , as the difference:

$$B = T_{no.bc} - T_{bc}.$$

[6] Biases vary spatiotemporally. To determine whether coherent and predictable patterns exist, both simple statistics and empirical orthogonal function (EOF) analyses were used [e.g., Davis, 1976]. The analyses were done on the monthly  $1^{\circ} \times 1^{\circ}$  AVHRR SST biases ( $B$ ) from January 1982 to December 2002. The EOF decomposition has the advantage of compressing data most efficiently using a few

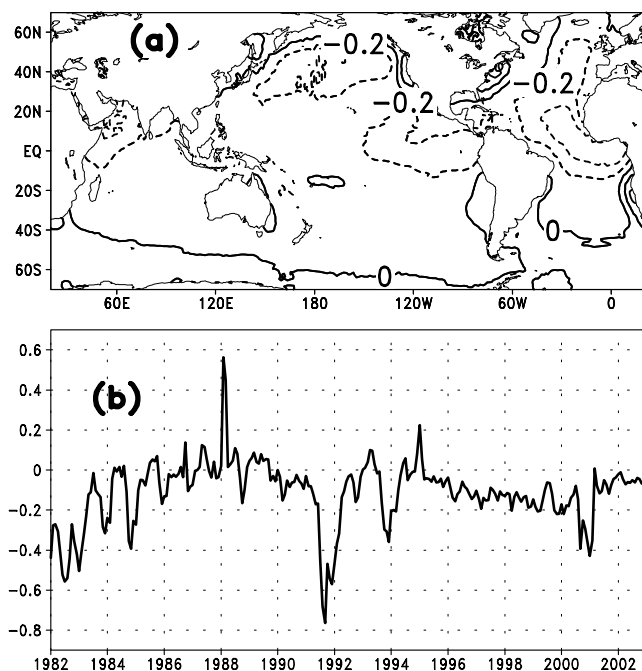


**Figure 2.** (a) Spatial pattern of the monthly AVHRR SST biases averaged January 1982–December 2002 (CI = 0.2; adjacent solid and dashed lines are 0 and  $-0.2^{\circ}\text{C}$  respectively). (b) Time series of the globally averaged AVHRR SST biases ( $^{\circ}\text{C}$ ). Time ticks indicate the beginning (January) of the year.

dominant spatiotemporal modes. Spatial projections of these modes reveal patterns, and temporal projections reveal sequences of events.

### 3. Results

[7] Figure 2a shows the 21-year averaged global bias, which was removed from the biases before the EOF decomposition. The largest biases are in the eastern tropical Atlantic following the shape of the coast. The persistent negative biases, with peaks larger than  $0.5^{\circ}\text{C}$ , are largely due to the dust aerosol from the African deserts. Negative biases also appear in the Arabian Sea. Positive biases, appearing along the east and west coasts of the United States (with maxima of  $0.3^{\circ}\text{C}$  and  $0.5^{\circ}\text{C}$ , respectively) and along the southwest coast of South Africa, are somewhat collocated with the cold waters along the coasts due to strong upwelling. The coastal biases may indicate the lack of in situ data used in tuning the satellite SST algorithms, or/and deficiencies in globally tuned SST algorithms, which is incapable of representing local conditions (see section 4 for more discussion).

[8] Figure 2b shows the temporal variation of the globally averaged biases. The biggest events in 1982/1983, 1991/1992 and 2000/2001 are due to El Chichón and Mt. Pinatubo eruptions [Reynolds, 1993] and the deteriorating performance of the NOAA-14 satellite at the end of its mission, respectively. Although the NOAA-16 satellite was launched in September 2000, new operational SST retrieval algorithms were not available until March 2001. This underscores the importance of overlapping satellite missions. The peaks in 1992–1995 were due to a satellite calibration error discussed in Reynolds [1993], which was fixed later. Note that during the quiet time, e.g., from March 1995 to mid 1999, the globally averaged bias increased from  $-0.05^{\circ}\text{C}$  to  $-0.20^{\circ}\text{C}$ . This indicates that at the start of the satellite mission the algorithm was well calibrated on a global average. However, large biases still occurred over certain regions, as shown in Figure 2a and further discussed below. The downward trend with time may indicate the shift of either the satellite orbit or the performance of the onboard SST instruments, or both. When the NOAA-16 satellite was operational for SST, the globally averaged bias dropped back to about  $-0.05^{\circ}\text{C}$  and was stable to the end of our analysis (December 2002).

[9] Figure 3 shows the percent variances of the first 25 EOFs. The variance decreases rapidly with mode num-

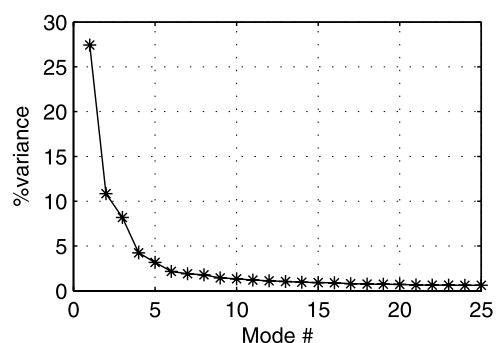


**Figure 3.** Percent variances of the first 25 modes on the AVHRR SST biases with mean removed.

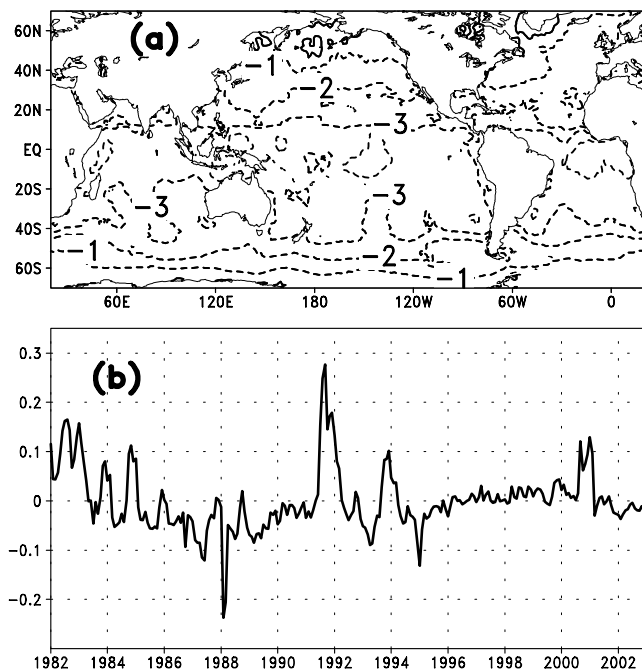


**Figure 4.** Mode #1 of the EOF decomposition on the AVHRR SST biases with the time mean removed: (a) spatial pattern (CI = 1; adjacent solid and dashed lines are 0 and -1 respectively); and (b) time series.

ber. Contributions from mode 1 to 6 are 27.4%, 10.8%, 8.2%, 4.2%, 3.2% and 2.2%, respectively. All other modes account for less than 2% individually. The higher modes have smaller spatial scales, indicating they are likely associated with errors and/or localized atmospheric phenomena.

[10] Figure 4 shows the spatial pattern (loading) and time series of Mode 1. The loading is largely zonal, with largest biases in the tropics. The time series is very close to that of the globally averaged biases (with a sign change), indicating that events in Mode 1 are global phenomena (volcano eruptions and satellite instrument decay).

[11] Mode 1 describes relatively rare events which are unpredictable. Fortunately these large biases can be easily identified and may be at least partially removed by special post-event algorithm changes. However, Mt. Pinatubo biases remain even in the post-processed Pathfinder AVHRR SST [Kilpatrick *et al.*, 2001], and the globally averaged Pathfinder SST biases are no less than that of the operational SST biases [Reynolds *et al.*, 2002]. In contrast to the rare events, regularly occurring biases could be removed or reduced by improvements to real time operational satellite algorithms. Examples of these biases are the mean biases described above and the seasonal biases described below.

[12] Figure 5 shows the loading patterns and time series of Mode 2 and 3 respectively. The time series show a robust seasonality, which is also shown in Mode 4. Positive peaks are in/near July for both Mode 2 and 3. Negative troughs are near November for Mode 2 and around April for Mode 3. Combining the time series with the spatial patterns of Mode 2, 3 and 4, we see negative biases in the northwestern Indian Ocean and the subtropical eastern Atlantic Ocean off of Africa in the northern summer (July). These negative biases are also consistent

with the patterns in the climate mean field (Figure 2a). They are likely associated with the dust aerosols in these regions during the northern summer. Aerosol induced biases are negative because the infrared radiation from sea surface was absorbed by the aerosol and then re-emitted at the aerosol's lower temperature [e.g., Reynolds, 1993]. Biases in the northern oceans are positive in July, revealing the algorithms' deficiency in these regions. These biases are co-located with the maximum and persistent cloud covers (e.g., cloud climatology at the International Satellite Cloud Climatology Project, <http://isccp.giss.nasa.gov/>), although there is no physical reason for positive

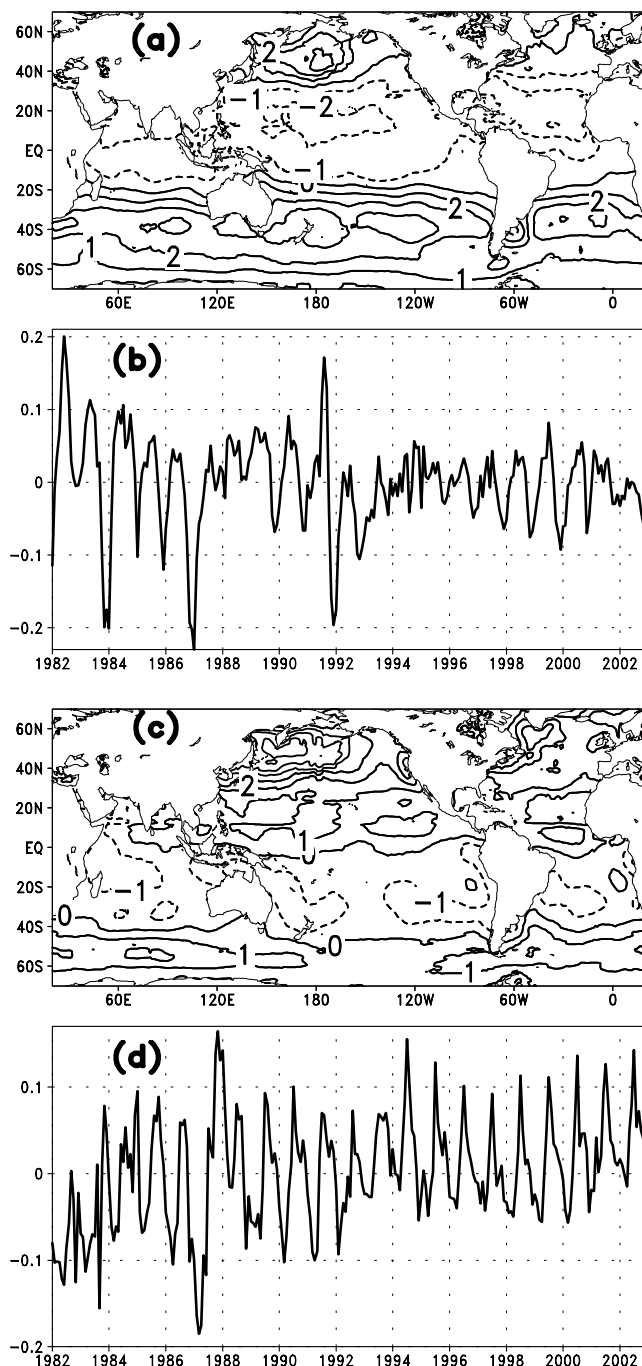


**Figure 5.** Same as Figure 4 but for Mode #2 (a, b) and #3 (c, d).

biases by clouds. This is likely linked to the deficiencies of globally tuned algorithms.

#### 4. Summary and Discussions

[13] Over the years the operational AVHRR SST retrieval algorithms have progressed from the early multi-channel linear retrieval to the current nonlinear retrieval. However all the algorithms are spatially independent. When a new satellite is launched, a new SST retrieval algorithm is developed and calibrated for its track and onboard instruments. The algorithm is then applied globally and remains the same during the lifetime of the satellite's mission unless major biases are identified (e.g., due to volcanic eruptions). In the latter cases special algorithms might be developed. We analyzed the statistical spatial and temporal patterns of the historical monthly AVHRR SST biases from January 1982 to December 2002, to assess the performance of the time- and space-independent operational AVHRR SST retrieval algorithms. Similar bias characterizations could be performed for other and recent satellite SST products.

[14] For the globally tuned algorithms, the global average biases were generally small. However, the biases were inhomogeneous and large in certain areas. Even in the 21-year climatological mean, the biases can be larger than 0.5°C. Areas with globally unrepresentative atmospheric thermal structure or aerosols showed greatest biases. Regions with atmospheric inversions and undetected warm clouds relative to the ocean surface emit more infrared radiance (IR) for a given SST. This results in positive AVHRR SST biases from a globally tuned algorithm. Likewise, regions or occasions with more aerosols than implicit in the global tuning emit less IR for a given SST, resulting negative biases. The spatial inhomogeneity of the biases indicates that spatially dependent satellite SST retrieval algorithms are necessary.

[15] In the time domain, Modes 2 to 4 showed strong seasonality and Mode 5 showed a trend in time (not shown). Time trends lasting several years were also revealed in the time series of the global mean and Mode 1. These indicate that time-dependent satellite SST retrieval algorithms may also be needed. The fact that coherent and regularly occurring patterns exist in the dominant modes is encouraging and useful. The seasonality could be used to guide improvements of the satellite SST algorithms with simplified time-dependence. The results have their implications for future satellite SST missions. The temporal patterns also showed the importance of overlapping satellite missions.

[16] The spatiotemporal bias patterns are apparently related to seasonal weather phenomena, such as the dust aerosols from the African deserts and the seasonal clouds over the northwest basins of North Pacific and North Atlantic Oceans. Proper parameterization of the retrieval sensitivity to these phenomena may also help to reduce the AVHRR SST biases.

[17] **Acknowledgments.** We thank Drs. Tom Peterson, Lei Shi and Sharon LeDuc for insightful comments and suggestions. Detailed comments from David Parker and an anonymous reviewer are greatly

appreciated. We are grateful to NCDC and the NOAA Office of Global Programs, which provided support for this work. The Grid Analysis and Display System (GrADS) developed at the Center for Ocean-Land-Atmosphere Studies [<http://grads.iges.org/grads>] was used for the plots.

#### References

- Brown, J. W., O. B. Brown, and R. H. Evans (1993), Calibration of advanced very high resolution radiometer infrared channels: A new approach to nonlinear correction, *J. Geophys. Res.*, **98**, 18,267–18,268.
- Davis, R. E. (1976), Predictability of sea surface temperature and sea level pressure anomalies over the North Pacific Ocean, *J. Phys. Oceanogr.*, **6**, 249–266.
- Donlon, C. J., P. J. Minnett, C. Gentemann, T. J. Nightingale, I. J. Barton, B. Ward, and M. J. Murray (2002), Toward improved validation of satellite sea surface skin temperature measurements for climate research, *J. Clim.*, **15**(4), 353–369.
- Emery, W. J., D. J. Baldwin, P. Schlüssel, and R. W. Reynolds (2001a), Accuracy of in situ sea surface temperatures used to calibrate infrared satellite measurements, *J. Geophys. Res.*, **106**, 2387–2405.
- Emery, W. J., S. Castro, G. A. Wick, P. Schlüssel, and C. Donlon (2001b), Estimating sea surface temperature from infrared satellite and in situ temperature data, *Bull. Amer. Meteorol. Soc.*, **82**(12), 2773–2786.
- Esaias, W. E., et al. (1998), An overview of MODIS capabilities for ocean science observations, *IEEE Trans. Geosci. Remote Sens.*, **36**, 1250–1265.
- Kent, E. C., P. K. Taylor, B. S. Truscott, and J. A. Hopkins (1993), The accuracy of voluntary observing ship's meteorological observations, *J. Atmos. Oceanic Tech.*, **10**, 591–608.
- Kent, E. C., P. G. Challenor, and P. K. Taylor (1999), A statistical determination of the random observational errors present in voluntary observing ships meteorological reports, *J. Atmos. Oceanic Tech.*, **16**, 905–914.
- Kilpatrick, K. A., G. P. Podesta, and R. Evans (2001), Overview of the NOAA/NASA advanced very high resolution radiometer Pathfinder algorithm for sea surface temperature and associated matchup database, *J. Geophys. Res.*, **106**(C5), 9179–9197.
- Kummerow, C., W. Barnes, T. Kozu, J. Shiue, and J. Simpson (1998), The Tropical Rainfall Measuring Mission (TRMM) sensor package, *J. Atmos. Oceanic Tech.*, **15**, 809–817.
- May, D. A., M. M. Parmeter, D. S. Olszewski, and B. D. McKenzie (1998), Operational processing of satellite sea surface temperature retrievals at the Naval Oceanographic Office, *Bull. Am. Meteorol. Soc.*, **79**, 397–407.
- McClain, E. P., W. G. Pichel, and C. C. Walton (1985), Comparative performance of AVHRR-based multichannel sea surface temperatures, *J. Geophys. Res.*, **90**, 11,587–11,601.
- Mutlow, C. T., A. M. Zavody, I. J. Barton, and D. T. Llewellyn-Jones (1994), Sea surface temperature measurements by the along-track scanning radiometer on the *ERS-1* satellite: Early results, *J. Geophys. Res.*, **99**, 2575–2588.
- Reynolds, R. W. (1993), Impact of Mount Pinatubo aerosols on satellite-derived sea surface temperatures, *J. Clim.*, **6**, 768–774.
- Reynolds, R. W., and T. M. Smith (1994), Improved global sea surface temperature analyses using optimum interpolation, *J. Clim.*, **7**, 929–948.
- Reynolds, R. W., N. A. Rayner, T. M. Smith, D. C. Stokes, and W. Wang (2002), An improved in situ and satellite SST analysis for climate, *J. Clim.*, **15**, 1609–1625.
- Walton, C. C. (1988), Nonlinear multichannel algorithms for estimating sea surface temperature with AVHRR satellite data, *J. Appl. Meteorol.*, **27**, 115–124.
- Walton, C. C., W. G. Pichel, J. F. Sapper, and D. A. May (1998), The development and operational application of nonlinear algorithms for the measurement of sea surface temperatures with the NOAA polar-orbiting environmental satellites, *J. Geophys. Res.*, **103**, 27,999–28,012.
- Wentz, F. J., C. L. Gentemann, D. K. Smith, and D. B. Chelton (2000), Satellite measurements of sea-surface temperature through clouds, *Science*, **288**, 847–850.

H.-M. Zhang, R. W. Reynolds, and T. M. Smith, NOAA NESDIS National Climatic Data Center, 151 Patton Avenue, Asheville, NC 28801, USA. ([huai-min.zhang@noaa.gov](mailto:huai-min.zhang@noaa.gov))